Subcutaneous gold nanorods detection with diffusion reflection measurement

Dror Fixler
Rinat Ankri

Subcutaneous gold nanorods detection with diffusion reflection measurement

Dror Fixler and Rinat Ankri
Bar-Ilan University, Faculty of Engineering and the Institute of Nanotechnology and Advanced Materials, Ramat-Gan, 52900, Israel

Abstract. The ability to quantitatively and noninvasively detect nanoparticles nearby the skin surface has important implications on their development as an *in vivo* cancer diagnostic tool. The diffusion reflection (DR) method is a simple, noninvasive imaging technique which has been proven useful for the investigation of the optical parameters of the tissue. A new method is presented for the measurements of gold nanorod (GNR) concentration in tissue-like phantoms, based on DR measurement and intense light absorption of GNR. Monte Carlo simulations and tissue-like phantom measurements of the reflected light intensity are presented. The ability to extract optical properties of phantoms and their GNR concentrations from DR measurements is demonstrated, followed by a discussion about the best mathematical model for light propagation in tissues, based on the diffusion theory. © *2013 Society of Photo-Optical Instrumentation Engineers (SPIE)* [DOI: 10.1117/1.JBO.18.6.061226]

1 Introduction

Nanoparticle-based contrast agents for molecular imaging have become a mainstay imaging tool for selectively detecting and imaging biological processes and diseases. Because of their nontoxicity to living cells,[1,2] biocompatibility, and favorable optical properties, such as an enhanced absorption cross-section[3] and adjustable scattering properties,[4] gold nanoparticles serve as promising agents for diagnostics and treatment of carcinoma. Therefore, the development of nanoparticle-based technologies for *in vivo* therapeutic and diagnostic application is under intensive study[5–7] and has been recently implemented in skin disease research.[8,9]

The many applications being developed based on skin surface irradiation for clinical or diagnostic purposes require an inherent understanding of photon migration in the tissue. Many researchers present the influence of optical tissue parameters on the light path inside the tissue.[10–14] A comprehensive study of different tissues, representing various spatial distributions of optical tissue components and their response to irradiated light, is still under investigation.[15–18]

One of the simplest tools that has been theoretically proven useful for the investigation of tissue optical parameters is the diffusion model for light path in irradiated tissue. This model enables the study of reflected light intensity (Γ) measurements from several distances on the tissue surface (ρ), from which deduction of the tissue optical properties, such as the absorption coefficient μ_a and the reduced scattering coefficient μ_s', is possible. Such a model predicts $\Gamma(\rho)$ for given values of μ_a and μ_s', making it possible to find the μ_a and μ_s' that give the best agreement between $\Gamma(\rho)$ and the measured data. In this paper, a model of light propagation is used, based on the diffusion theory in a homogeneous, infinite medium.[19] As was previously discussed

by Farrell et al.,[19] the $\Gamma(\rho)$ function can be described by the general equation

$$\Gamma(\rho) = \frac{C_1}{(\rho)^m} \, \exp(-\mu\rho), \qquad (1)$$

where C_1 is a constant depending on the optical properties of the medium and the sizes of the source and detector apertures. μ is the effective attenuation coefficient given by (for $\mu_a \ll \mu_s'$)[19,20]

$$\mu = \sqrt{3 \cdot \mu_a \mu_s'}, \qquad (2)$$

where m is the power of ρ, which depends on ρ's range, as well as on the scattering properties[19,21] and the absorption properties of the tissue. Equation (1) can be rewritten as

$$\ln[\rho^m \Gamma(\rho)] = c_2 - \mu \cdot \rho. \qquad (3)$$

Equation (3) presents a linear correlation between $\ln[\rho^m \Gamma(\rho)]$ and μ. Resulting from Eq. (2), the square slope of the linear curve depends on the product between the absorption and the reduced scattering coefficient of the tissue.

Very recently, a new method has been suggested by us for cancer detection, based on the diffusion reflection (DR) measurement of gold nanorod (GNR).[22,23] Intensity-based DR measurements detected head and neck cancer cells adjacent to the skin surface.

In the current paper, we first examine which m best fits our experimental data from the DR measurement of solid phantoms simulating skin properties (since previous works suggest either $m = 1$[24–26] or $m = 2$,[27,28] as will be discussed). Once the appropriate m was defined, phantoms with GNR were irradiated and their DR profile was analyzed to obtain the GNR absorption coefficient and concentration in the phantom.

Address all correspondence to: Dror Fixler, Bar-Ilan University, Faculty of Engineering and the Institute of Nanotechnology and Advanced Materials, Ramat-Gan, 52900, Israel. Tel: +972-3-5317598; Fax: +972-3-7384050; E-mail: Dror.Fixler@biu.ac.il

2 Materials and Methods

2.1 Monte Carlo Simulation of Reflected Light Intensity from Irradiated Tissue

In order to substantiate and extend our experimental results, a Monte Carlo (MC) simulation of photon migration within irradiated tissue mimicking the skin surface optical properties was developed under the assumptions presented in Ankri et al.[23] Briefly, a turbid three-dimensional medium was defined according to a specific scattering coefficient μ_s, anisotropy factor g, and varying absorption coefficients μ_a. The reduced scattering coefficient was calculated by the following equation:

$$\mu_s' = (1 - g)\mu_s. \tag{4}$$

The simulation was performed for various absorption coefficients $\mu_a = 0.0115, 0.0126, 0.0182,$ and 0.0227 mm^{-1}, but with a constant reduced scattering coefficient $\mu_s' = 1.6 \text{ mm}^{-1}$. Photons were launched without reflection, perpendicular to the surface into a single point on the lattice plane $x = y = z = 0$. For each photon, the direction after a step of $dr = 250 \text{ }\mu\text{m}$ was calculated according to the scattering and absorption properties of the turbid medium. If the photon survived, its new location was calculated. When photons returned to the surface $z = 0$ they were ejected from the system.

The locations at which the photons reached the lattice surface $(x, y, 0)$ were recorded. The simulation displayed the radial distribution of reflected photons around the injection point to perform simulated $\ln[\rho\Gamma(\rho)]$ and $\ln[\rho^2\Gamma(\rho)]$ curves for the different absorption coefficients, for $m = 1$ and $m = 2$ of Eq. (3), correspondingly.

2.2 Experimental Set-Up

A noninvasive optical technique was designed and built (NEGOH-OP Technologies, Israel) for reflected light intensity measurements, as was previously described by us.[29] The set-up included a laser diode with a wavelength of 650 nm as an excitation source. Irradiation was carried out using a 125 μm diameter optic fiber to achieve a pencil beam illumination. We used a portable photodiode as a photo detector. The photodiode was placed at various distances ρ on the sample surface in order to enable $\Gamma(\rho)$ measurements. The photodiode was kept in close contact with the tissue surface to prevent ambient light from entering the detection system and to avoid potential light loss through specimen edges. The initial distance ρ between the light source and the first photodiode was ~1 mm. A consecutive reflected light intensity measurement was enabled using a micrometer plate which was attached to the optical fiber. The micrometer plate was moved by incremental steps of 250 μm each. As a result, the reflected light intensity was collected from 20 source-detector distances with ρ varying between 1 mm and 6 mm. The reflected intensity $\Gamma(\rho)$, presenting units of Volt per mm, was collected using a digital scope (Agilent Technologies, Mso7034a, Santa Clara, California) and data were processed using MATLAB.

A spatially modulated quantitative spectroscopy (SMoQS) instrument was used for the investigation of the phantoms' optical properties.[30] A noncontact, spectroscopic instrument utilized spatial frequency domain (SFD) modulated reflectance data to extract quantitative absorption (μ_a) and reduced scattering (μ_s') coefficients. The principles underlying the extraction of absorption and reduced scattering coefficient values using an SFD approach have recently been detailed elsewhere.[31]

2.3 Gold Nanorod Fabrication

GNR were synthesized using the seed mediated growth method.[32] A solution of GNR suspended in cetyltrimethylammonium bromide (CTAB) (SigmaAldrich, USA) was centrifuged at 11,000 g for 10 min, decanted, and resuspended in water to remove excess CTAB. The GNR size, shape, and uniformity were characterized using transmission electron microscopy and the resultant dimensions were 25×65 nm, with a narrow size distribution (10%).[23] Their absorption spectrum presented a high absorption peak in the wavelength of 650 nm (see Fig. 1).

2.4 Solid Phantoms

Solid phantoms with various absorption coefficients were prepared in order to simulate skin tissue with different optical properties.[33,34] The phantoms were prepared using varying concentrations of India ink 0.1% as an absorbing component and a constant concentration of Intralipid (IL) 20% as a scattering component (Lipofundin MCT/LCT 20%, B. Braun Melsungen AG, Germany). Agarose powder 1% (SeaKem LE Agarose, Lonza, USA) was added in order to convert solution into gel. The absorption spectrum of the India ink was determined using a spectrophotometer and the absorption coefficient of each phantom was calculated according to the concentration of the ink in each solution. All phantoms presented the same scattering properties using 2% of IL (this concentration refers to the solid fraction in the examined solution). The phantom solutions were heated and mixed at a temperature of approximately 90°C while the Agarose powder was slowly added. The phantom solutions were then poured into cell culture plates (90 mm) and cooled under vacuum conditions (to avoid bubbles).

Five different phantoms were measured. The ink concentrations were 2, 2.5, 3, 5, and 7 (%). The resultant absorption properties of the phantoms were 0.0115, 0.0126, 0.0137, 0.0182, and 0.0227 mm^{-1}. In addition, GNR (3.1 mg/ml) were added to a phantom solution containing 3% ink and 2% of IL, to simulate a tissue containing GNR.
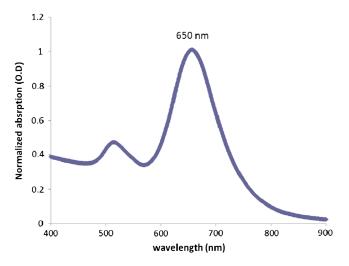

Fig. 1 GNR (25×65 nm) UV-vis absorption spectra (normalized).
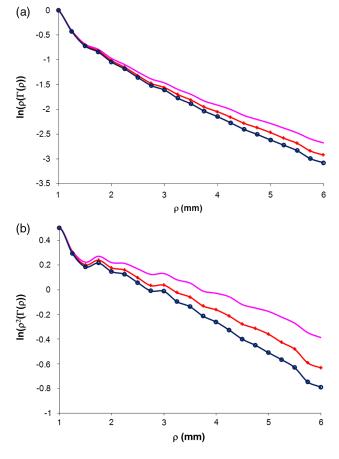
2.5 In Vivo Experiment

Our new method for tumor detection was evaluated using mice bearing human head and neck cancer derived from an A-431 squamous cell carcinoma (SCC) cell line.[22] A-431 cells (2×10^6) were injected subcutaneously into the back flank area of 10 to 11 week-old nude mice. When the tumor size reached a size of 7 to 9 mm in diameter, the mice received 100 μL (25 mg/ml) of immuno-targeted GNR by tail vein injection.[23] Mice tumor and normal tissue were scanned immediately after GNR injection and up to 10 h post injection. All *in vivo* measurements were performed under appropriate anesthesia.

3 Results

3.1 Simulations

The simulated reflected light intensity of four skin tissues which differ by their absorption coefficients (but present a constant scattering coefficient $\mu_s' = 1.6$ mm^{-1}) is presented in Fig. 2. The simulations were performed according to the description in Sec. 2.1.

Figure 2(a) presents the DR profiles plotted as the logarithm of the product between the distance and the reflectance, $\ln[\rho \cdot \Gamma(\rho)]$, versus the distance, for three representative tissues with a constant scattering coefficient but varying absorption coefficients $\mu_a = 0.0126$, 0.0182, and 0.0227 mm^{-1}. Figure 2(b)
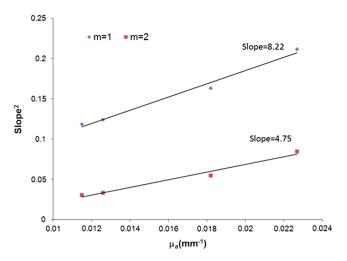

(a)

(b)

Fig. 2 DR simulation results for tissues presenting a constant reduced scattering coefficient of 1.6 mm^{-1} with three different absorption coefficients: 0.0126 mm^{-1} (solid line), 0.0182 mm^{-1} (+signs), and 0.0227 mm^{-1} (circles). (a) Simulated $\ln[\rho \cdot \Gamma(\rho)]$ profiles. (b) Simulated $\ln[\rho^2\Gamma(\rho)]$ profiles of the homogeneous tissues.

presents the DR profiles, of the same tissues, plotted as the logarithm of the product between the square distance and the reflectance $\ln[\rho^2\Gamma(\rho)]$ versus the distance. For both $m = 1$ and $m = 2$, the simulation results present the predicted dependence of the reflected light intensity profile on the lattice absorption coefficient: the higher the absorption coefficient, the sharper the decay of the reflected light intensity profile. Hence, the slope that is defined as the y-axis {the $\ln[\rho^m\Gamma(\rho)]$} divided by x-axis (the distance ρ) should yield the absorption of the irradiated sample. As can be seen in Fig. 2, the linear slope starts around 2.5 mm where the collimated light is less relevant and the diffusive regime starts.

The square slopes of these DR profiles are presented in Fig. 3. As was mentioned in the Introduction, according to the diffusion theory, the square slope of the DR curve is proportional to the product $3\mu_a\mu_s'$ [see Eq. (2)]. Therefore, the linear fit between the square slope and the absorption coefficient should yield the scattering coefficient of the sample (multiplied by 3 and with a constant difference of c_2). The linear fit for $m = 1$ presented a slope of 8.22 while the linear fit for $m = 2$ presented a slope of 4.75. The deviation of these slopes with 3 should yield the scattering coefficient of the samples. The resultant μ_s' for $m = 1$ is 2.4 mm^{-1} and for $m = 2$ is 1.58 mm^{-1}. As the reduced scattering coefficient inserted into the simulation parameters was 1.6 mm^{-1}, the resultant μ_s' for $m = 2$ is almost identical to it, while the resultant μ_s' for $m = 1$ is not. These simulation results suggest that the resultant curve slope of the DR profile of a tissue, plotted in the logarithmic form $\ln[\rho^2\Gamma(\rho)]$, is proportional to $\sqrt{3\mu_a\mu_s'}$ of an irradiated tissue.

In our previous publication in the *Journal of Biomedical Optics*,[29] we have shown that for multilayers tissues, (as in skin) when the absorption of the bottom layer is greater than the absorption in the upper layer, the $\ln[\rho^2\Gamma(\rho)]$ profile exhibits a single-layer behavior, albeit with an effective average absorption. Therefore, a model describing light propagation in homogeneous tissues is also suitable for the skin.
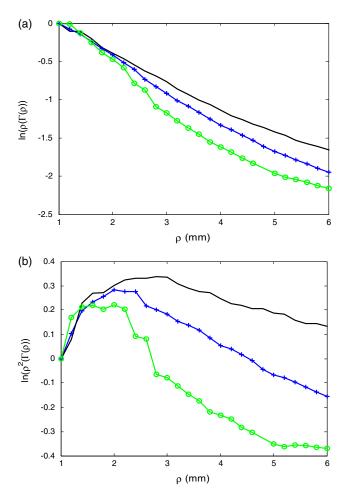

Fig. 3 The linear dependence of the square slope, on the absorption coefficients for the resulted curves presented in Fig. 2. The upper line presents the simulated linear curve for $\ln[\rho \cdot \Gamma(\rho)]$ square slopes and the bottom line presents the simulated linear curve for $\ln[\rho^2\Gamma(\rho)]$. Each square slope was calculated according to Eq. (3). The resultant slope of each linear fitting is presented at the end of each line. These simulation results demonstrate that the absorption coefficient of the tissue can be directly calculated from the slope of the diffusion reflection $\ln[\rho^2\Gamma(\rho)]$ curve.

3.2 DR Measurements of Solid Phantoms

The reflected light intensity from five different solid phantoms was measured using the experimental set-up described in Sec. 2.2 above. Representative results of the reflected light intensity profiles are presented in Fig. 4.

Figure 4(a) presents the DR profiles plotted as the logarithm of the product between the distance and the reflectance $\ln[\rho \cdot \Gamma(\rho)]$ versus the distance, for three representative phantoms with a constant scattering coefficient (2% IL) but varying absorption coefficients $\mu_a = 0.0137, 0.0182$, and 0.0227 mm^{-1}. Figure 4(b) presents the DR profiles of the same phantoms plotted as the logarithm of the product between the square distance and the reflectance $\ln[\rho^2 \Gamma(\rho)]$ versus the distance. The square slopes of these DR profiles, as well as of two additional phantoms presenting $\mu_a = 0.0115$ and 0.0126 mm^{-1}, are shown in Fig. 5. As was mentioned in the Introduction, according to the diffusion theory the square slope of the DR curve plotted as $\ln[\rho^m \Gamma(\rho)]$ minus a constant value of c_2 should be proportional to the product $3\mu_a \mu_s'$. Therefore, the linear fit between the square slope and the absorption coefficient should be proportional to the scattering coefficient of the sample. The linear fit for $m = 1$ presented a slope of 8.75 while the linear fit for $m = 2$ presented a slope of 4.52. By the deviation of these slopes with 3, one should get the scattering coefficient of the samples. The predicted scattering coefficient for 2% of IL is ~ 1.65 mm^{-1}[35] and the resultant μ_s' for $m = 1$ is 2.91 mm^{-1} and for $m = 2$ is 1.5 mm^{-1}. While the resultant reduced scattering coefficient for $m = 1$ is quite far from the predicted μ_s' of a phantom containing 2% IL, the resultant μ_s' for $m = 2$ is very similar to it. These experimental results suggest that the resultant curve slope of the DR profile of a tissue, plotted in the logarithmic form $\ln[\rho^2 \Gamma(\rho)]$, is proportional to $\sqrt{3\mu_a \mu_s'}$. These results match the values shown via simulation in Sec. 3.1.

3.3 Optical Properties of Phantoms Containing GNR

An SMoQS instrument was used for the determination of the phantoms' optical properties. The resulting absorption and reduced scattering coefficients of the phantoms with and without GNR, in the wavelength range of 450 to 900 nm, are presented in Fig. 6. In Fig. 6(a) one can notice the absorption peaks of the phantom with GNR in 530 and 650 nm, correlated to the absorption peaks of the suspended GNR (see Fig. 1). The absorption spectra of the base phantoms (phantoms without GNR) are also presented and it is well seen that their absorption properties are significantly lower and missing the characterization of the GNR. These results suggest that the absorption properties of the GNR are kept within the phantom. As the scattering properties are concerned [see Fig. 6(b)], the reduced scattering coefficients of these GNR in the near infrared region show no unique wavelength dependence (no peak that characterizes the GNR) and more importantly, their scattering properties are not different from the basic phantoms scattering spectrum. This is in contrast to other GNR sizes and shapes that might present a unique scattering spectrum.[4] Therefore, the GNR scattering properties can be negligible in this research compared to their absorption properties in the tissue.
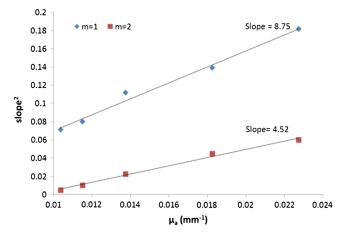

Fig. 4 DR measurement results for skin tissue-like phantoms presenting a constant reduced scattering coefficient (2% IL) with three different absorption coefficients: 0.0137 mm^{-1} (solid line), 0.0182 mm^{-1} (+ signs), and 0.0227 mm^{-1} (circles). (a) Experimental $\ln[\rho \cdot \Gamma(\rho)]$ profiles. (b) Experimental $\ln[\rho^2 \Gamma(\rho)]$ profiles of the homogeneous tissues.

Fig. 5 The linear dependence of the square slopes on the absorption coefficients of the samples for the resulted curves presented in Fig. 4. The upper line presents the experimental linear curve for $\ln[\rho \cdot \Gamma(\rho)]$ square slopes and the bottom line presents the experimental linear curve for $\ln[\rho^2 \Gamma(\rho)]$. The resultant linear slope of each linear fitting is presented at the end of each line.

3.4 DR Measurement of Solid Phantoms Containing GNR

Figure 7 shows representative results for the DR measurements plotted as $\ln[\rho^2\Gamma(\rho)]$ of two solid phantoms. The first phantom (circles, named as "A") contains 3% ink but no GNR. The second phantom (+signs, named as "B") contains 3% ink and 0.01 mg/mL of GNR. One can notice that the presence of GNR in the phantom increased the reflectance graph slope. Since GNR in this shape and size (an aspect ratio of 2.6 and an effective radius of ~19 nm[23]) have negligible scattering properties, the increase in the slope is due to the absorption properties of the GNR. Thus, from this slope one can calculate the absorption coefficient of the phantom, as its scattering coefficient was calculated in Sec. 3.2 above ($\mu_s' = 1.5$ mm^{-1}). In particular, in order to calculate the GNR concentration in the phantom, the Δ slope between the DR profiles of B and A should be considered. Since the ink concentrations in A and B were the same, this Δ slope arises from the presence of the GNR and therefore indicates the GNR absorption coefficient in the phantom. By dividing the resultant absorption coefficient with the GNR extinction coefficient, which was found to be ~1 ml/(mm * mg),[23] the GNR concentration in the phantom was calculated as follows:
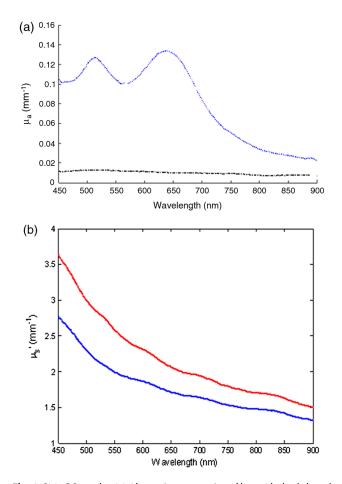
1. The resulted Δ slope in Fig. 7 was 0.08.

2. The linear correlation between the square slopes and the absorption coefficients of the phantom, was found to be equal to 4.52.

Thus, the resulting GNR absorption coefficient in phantom B was 0.014 mm^{-1}. Dividing this μ_a with the GNR extinction coefficient, the resultant GNR concentration in the phantom is 0.014 mg/mL, very similar to the predicted $\mu_a = 0.01$ mm^{-1}. Using the comparison method, the constant c_2 is not relevant anymore.
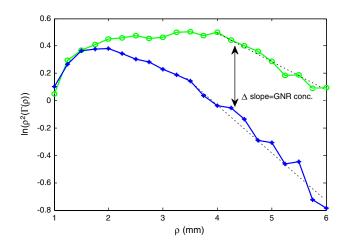
Following the fact that *in vivo* measurements deal with multilayer situations, we put upper silicon phantom layer on top of the GNR phantoms with different thicknesses of 3, 4, 5, 6.3, 7.8, 9.5, 11.1, 14.1, and 17 mm. These phantoms were measured and the absorption coefficient of the two layers (measured as a single unit) was extracted. Figure 8 shows the absorption coefficients of the two layers unit as a percentage of the absorption coefficient of the upper layer [μ_a of (GNR phantom + the upper layer)/μ_a of the upper layer]. Figure 8 presents these results in 656 nm for two phantoms with 0.02 and 0.135 mg/ml of GNR. The average absorption coefficient of the upper layer in the range of 650 to 750 nm was $\mu_a = 0.02$ mm^{-1} and its average reduced scattering coefficient was $\mu_s = 1.1$ mm^{-1}. The addition of a GNR phantom as a bottom layer increased the measured absorption coefficient. This incensement changes according to the upper layer thickness: the thinner the upper layer is the larger the incensement. Thus, the %absorption decreases from ~1030% to ~114% (for the highest absorbing GNR). Based on these results we show that one can detect the GNR presence even in a multilayer situation.
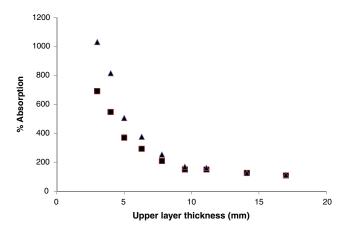
3.5 In Vivo Results

Our suggested method must fit the heterogeneous properties of tissues. In order to test the possibility of using the new method in practice, tumor-bearing mice were irradiated, under appropriate anesthesia, and the reflected light intensity was measured. The idea is to look for the increase in the absorption properties

Fig. 6 SMoQS results. (a) Absorption properties of base (dashed-dotted line) and 0.135 mg/ml GNR (dotted line) phantoms. (b) Scattering properties of 0.135 mg/ml GNR (blue line) and base (red line). The absorption spectrum of the GNR is well seen, indicating the preservation of the GNR optical properties within the phantoms.

Fig. 7 Experimental results for DR measurements of a phantom containing 3% ink and 2% IL compared to the DR results for the same phantom with an added 0.01 mg/mL GNR. Based on the facts that the $\ln[\rho^2\Gamma(\rho)]$ slope is equal to $\mu = \sqrt{3 \cdot \mu_a\mu_s'}$, that the GNR scattering at 650 nm is negligible, and that μ_a can be translated to the GNR concentration using their extinction coefficient, the GNR concentration in the phantom can be calculated from the Δslope between the two presented curves.

Fig. 8 %Absorption measurements of phantoms with GNR with upper Si phantom layers presenting different thicknesses of 3, 4, 5, 6.3, 7.8, 9.5, 11, 14, and 17 mm measured in two GNR concentrations of 0.02 mg/ml (squares) and 0.135 mg/ml (triangulars).

following the GNR insertion into real tissue. The reflectance measurements were performed before the GNR injection, immediately after injection, and 10 h post injection. The slopes of the reflected light intensity profiles were calculated and representative results are shown in Fig. 9. In order to take into consideration the fact that the tissue's native absorption coefficient may vary due to the variance in blood concentration, especially when there are tumors under the skin, we did two control measurements: (1) skin without tumor and (2) the tumor before injecting the GNR. Thus, while extracting the GNR concentration based on the Δ slope, both controls cancel the variance in blood concentration.

Figure 9 compares between the reflected light intensity slopes (absolute values) of the cancerous (black columns) and the normal tissues (white columns), for three representative times: (1) before GNR injection; (2) immediately after intravenous injection; and (3) more than 10 h post injection. It is clearly demonstrated that the absorption properties can be seen in a heterogeneous environment. There is no way to find a difference between the tumor and the normal tissue before the injection. In contrast, ten hours post GNR injection there is a significant change (of more than 50%) between the reflectance profiles of

Fig. 9 Comparison between the reflected light intensity slopes (absolute values) of the cancerous (black columns) and normal (white columns) tissues at several time points. Absolute values of the slope, for a each mouse, are presented. The results are the average of five to ten diffusion reflection measurements of different mice. The error bars represent error of the mean.

the cancerous and of the normal tissue. This change results from specific accumulation of GNR in the tumor. We also demonstrated that immediately after GNR injection, the reflectance profiles of both the cancerous and the normal tissues represent an increase in their slopes, which indicates the GNR circulating time in the blood. This clear discrimination between cancerous and normal tissue enables sensitive and specific skin cancer detection based on GNR enhanced diffusion reflection measurements.

4 Discussion and Summary

The dependence of the reflected light intensity profile on the skin optical properties has been intensively discussed.[12–14,20] The above described photon migration model presents a very simple tool for the deduction of optical skin properties using reflected light intensity analyses.

In the present study, the diffusion model for light path within irradiated skin tissue was used for the extraction of skin tissue optical properties. This theory suggests two main approaches for the reflected light intensity profile analyses, for $m = 1$ and for $m = 2$, which depend on the range of ρ, the optical properties of the tissue, and the optical set-up aperture.

In order to find which power (m) of ρ best correlates between our DR measurements and the optical properties of an irradiated skin tissue, MC simulations and phantom experiments were performed. Simulation results exhibit a high correlation to the reflectance equation [Eq. (1)] for $m = 2$, since the tissue scattering coefficient was extracted from the graph slope using Eq. (2). This result was also observed in experimental results from tissue-like phantoms, since the scattering coefficient resulting from the slope of $\ln\left[\rho^2\Gamma(\rho)\right]$ curves was 1.52 mm^{-1}, very similar to the expected scattering coefficient for 2% IL.[35]

DR is usually described by the insertion of $m = 1$ to Eq. (1). Venugopalan et al.[36] presented an analytical work suggesting that for a high scattering media (which better correlates the diffusion behavior) far from the light source (experimental results were presented for $0 < \rho < 32$ mm), $m = 1$. In a high absorbing media, m was found to be equal to 2, but only pertaining to collimated light since diffusive light is much less dominant under conditions of high absorbance. Zaccanti et al.[25] presented experimental results for $\mu_s' > 1$ mm^{-1} and μ_a less than 0.3% of the μ_s', which best fitted $m = 1$ in the range of $10 < \rho < 35$ mm. Also, Zhang et al.[37] discussed phantom experiments which best fitted $m = 1$ for absorbing media presenting $0.02 < \mu_a < 0.12$ mm^{-1} and 3.2% of the scattering component (IL 10%) in the range of $\sim4 < \rho < 60$ mm. All these works present DR measurements in relatively large source-detector separations ($10 < \rho < 30$ mm, on average). Our results suggest that DR measurement in relatively small values of ρ ($1 < \rho < 6$ mm) fit the general Eq. (1) but with the power of $m = 2$, which is more familiar from the random walk approximation[38] (which can also pertain to collimated light as stated above[36]). Gandjbakhche and Weiss[27] also found a linear fit for $m = 2$ at $9 < \rho < 11$ mm. Further investigation is required in order to better understand light paths in small source-detector distances.

Anyway, the DR profiles were successfully analyzed as the optical properties of the samples were extracted. A phantom mimicking skin properties containing GNR was irradiated and its reflection curve was plotted in the logarithmic form $\ln\left[\rho^2\Gamma(\rho)\right]$. The GNR presented in this paper have high absorption at 650 nm but negligible scattering. Therefore, the increase in the DR profile resulted from the GNR absorption properties. Thus, from the $\ln\left[\rho^2\Gamma(\rho)\right]$ slope, the absorption coefficient of the phantom was deduced.

Using the extinction coefficient of the GNR, their concentration in the skin like phantom was measured.

The results presented in this article suggest that from the DR profile one can extract optical skin tissue properties by plotting the DR intensity in the logarithmic form $\ln[\rho^2\Gamma(\rho)]$. Since GNR can be regarded as an additional absorption component in the tissue, its concentration can be calculated from the $\ln[\rho^2\Gamma(\rho)]$ DR profile of the irradiated tissue. These results are highly important since GNR can be specifically targeted to tumors in the skin layer, and thus may be used for tumor detection. In addition, GNR concentration in a tumor can serve as a simple parameter indicating tumor size.

In summary, the results in this paper prove that DR measurements can be used for the calculation of GNR concentration in skin tissue. This preliminary research paves the way for further study of the DR method for tumor detection.

Acknowledgments

References

1. M. Eghtedari et al., "Engineering of hetero-functional gold nanorods for the *in vivo* molecular targeting of breast cancer cells," *Nano Lett.* **9**(1), 287–291 (2009).
2. G. von Maltzahn et al., "Computationally guided photothermal tumor therapy using long-circulating gold nanorod antennas," *Cancer Res.* **69**(9), 3892–3900 (2009).
3. M. A. El-Sayed, "Some interesting properties of metals confined in time and nanometer space of different shapes," *Acc. Chem. Res.* **34**(4), 257–264 (2001).
4. P. K. Jain et al., "Calculated absorption and scattering properties of gold nanoparticles of different size, shape, and composition: applications in biological imaging and biomedicine," *J. Phys. Chem. B* **110**(14), 7238–7248 (2006).
5. J. A. Copland et al., "Bioconjugated gold nanoparticles as a molecular based contrast agent: implications for imaging of deep tumors using optoacoustic tomography," *Mol. Imag. Biol.* **6**(5), 341–349 (2004).
6. J. F. Hainfeld et al., "Gold nanoparticles: a new X-ray contrast agent," *J. Radiol.* **79**(939), 248–253 (2006).
7. R. Popovtzer et al., "Targeted gold nanoparticles enable molecular CT imaging of cancer," *Nano Lett.* **8**(12), 4593–4596 (2008).
8. Q. Zhang et al., "Gold nanoparticles as a contrast agent for *in vivo* tumor imaging with photoacoustic tomography," *Nanotechnology* **20**(39), 395102–395109 (2009).
9. T. J. Robinson et al., "High performance *in vivo* near-IR (>1 μm) imaging and photothermal cancer therapy with carbon nanotubes," *Nano Res.* **3**(11), 779–793 (2010).
10. G. H Weiss, "Statistical properties of the penetration of photons into a semi-infinite turbid medium: a random-walk analysis," *Appl. Opt.* **37**(16), 3558–3563 (1998).
11. G. Zaccanti et al., "Method for measuring the mean time of flight spent by photons inside a volume element of a highly diffusing medium," *Opt. Lett.* **24**(18), 1290–1292 (1999).
12. S. Del Bianco, F. Martelli, and G. Zaccanti, "Penetration depth of light re-emitted by a diffusive medium: theoretical and experimental investigation," *Phys. Med. Biol.* **47**(23), 4131–4144 (2002).
13. L. Dagdug, G. H. Weiss, and A. H. Gandjbakhche, "Effects of anisotropic optical properties on photon migration in structured tissues," *Phys. Med. Biol.* **48**(10), 1361–1370 (2003).
14. X. Guo, M. F. G. Wood, and A. Vitkin, "A Monte Carlo study of penetration depth and sampling volume of polarized light in turbid media," *Opt. Comm.* **281**(3), 380–387 (2008).
15. T. H. Pham et al., "Quantifying the absorption and reduced scattering coefficients of tissue like turbid media over a broad spectral range with noncontact Fourier-transform hyperspectral imaging," *Appl. Opt.* **39**(34), 6487–6497 (2000).
16. A. M. Maiorova et al., "Fiber-optic backscattering profile measurements for determination of the optical coefficients of turbid media," *J. Russ. Las. Res.* **24**(1), 1–13 (2003).
17. A. Sviridov et al., "Intensity profiles of linearly polarized light backscattered from skin and tissue-like phantoms," *J. Biomed. Opt.* **10**(1), 014012 (2005).
18. A. Garcia-Uribe et al., "In-vivo characterization of optical properties of pigmented skin lesions including melanoma using oblique incidence diffuse reflectance spectrometry," *J. Biomed. Opt.* **16**(2), 020501 (2011).
19. T. J. Farrell, M. S. Patterson, and B. Wilson, "A diffusion theory model of spatially resolved, steady-state diffuse reflectance for the noninvasive determination of tissue optical properties *in vivo*," *Med. Phys.* **19**(4), 879–888 (1992).
20. S. T. Jacques and B. W. Pogue, "Tutorial on diffuse light transport," *J. Biomed. Opt.* **13**(4), 041302 (2008).
21. R. Ankri, H. Taitelbaum, and D. Fixler, "On phantom experiment of the photon migration model in tissues," *Open Opt. J* **5**(Suppl. 1-M4), 28–32 (2011).
22. R. Ankri et al., "A new method for cancer detection based on diffusion reflection measurements of targeted gold nanorods," *Int. J. Nanomed.* **7**, 449–455 (2012).
23. R. Ankri et al., "In-vivo tumor detection using diffusion reflection measurements of targeted gold nanorods—a quantitative study," *J. Biophoton.* **5**(3), 263–273 (2012).
24. J. M. Schmitt et al., "Multi layer model of photon diffusion in skin," *J. Opt. Soc. Am. A.* **7**(11), 2141–2153 (1990).
25. G. Zaccanti, S. Del Bianco, and F. Martelli, "Measurements of optical properties of high-density media," *Appl. Opt.* **42**(19), 4023–4030 (2003).
26. P. Di Ninni, F. Martelli, and G. Zaccanti, "Toward a reference standard for tissue phantoms," *Proc. SPIE* **7906**, 79060M (2011).
27. A. H. Gandjbakhche and G. H. Weiss, "Random walk and diffusion-like models of photon migration in turbid media," *Prog. Opt.* **34**, 333–402 (1995).
28. P. A. Weersink et al., "Accuracy of noninvasive *in vivo* measurements of photosensitizer uptake based on a diffusion model of reflectance spectroscopy," *Photochem. Photobio.* **66**(3), 326–335 (1997).
29. R. Ankri, H. Taitelbaum, and D. Fixler, "Reflected light intensity profile of two-layer tissues: phantom experiments," *J. Biomed. Opt.* **16**(8), 085001 (2011).
30. A. J. Lin et al., "Spatial frequency domain imaging of intrinsic optical property contrast in a mouse model of alzheimer's disease," *Ann. Biomed. Eng.* **39**(4), 1349–1357 (2011).
31. R. B. Saager, D. J. Cuccia, and A. J. Durkin, "Determination of optical properties of turbid media spanning visible and near-infrared regimes via spatially modulated quantitative spectroscopy," *J. Biomed. Opt.* **15**(1), 017012 (2010).
32. B. Nikoobakht and M. A. El-Sayed, "Preparation and growth mechanism of gold nanorods (nrs) using seed-mediated growth method," *Chem. Mater.* **15**(10), 1957–1962 (2003).
33. J. S. Dam et al., "Fiber-optic probe for noninvasive real-time determination of tissue optical properties at multiple wavelengths," *Appl. Opt.* **40**(7), 1155–1164 (2001).
34. C. Yaqin et al., "Determination of tissue optical properties from spatially resolved relative diffuse reflectance by PCA-NN," in *IEEE Int. Conf. Neural Networks & Signal Processing* Vol. 1, pp. 369–372, IEEE, Nanjing, China (2003).
35. R. Cubeddu et al., "A solid tissue phantom for photon migration studies," *Phys. Med. Biol.* **42**(10), 1971–1979 (1997).
36. V. Venugopalan, J. S. You, and B. J. Tromberg, "Radiative transport in the diffusion approximation: an extension for highly absorbing media and small source-detector separations," *Phys. Rev. E* **58**(2), 2395–2407 (1998).
37. L. S. Zhang et al., "Measurements of absorption and anisotropy coefficients of the fat emulsion intralipid-10%," *Chin. Phys. Lett.* **21**(12), 2517–2520 (2004).
38. R. F. Bonner et al., "Model for photon migration in turbid biological media," *J. Opt. Soc. Am.* **4**(3), 423–432 (1987).